Contactless Characterization of Silicon Wafers

Dieter K. Schroder

Department of Electrical Engineering/Center for Solid State Electronics Research
Arizona State University, Tempe, AZ 85287-5706, USA

Abstract

Contactless measurements are attractive and more commonly used because they do not contaminate the sample and generally do not require sample preparation. After an outline of the more common contactless characterization techniques, I will discuss a few of these in more detail. In particular resistivity or doping density profiling, minority carrier lifetime, stress, temperature, layer thickness, and critical dimension will be more fully described.

Introduction

A summary of the major *contactless* characterization techniques is shown here. A few of these techniques are discussed in more detail.

Resistivity	Eddy current, capacitance-voltage, corona charge, photoluminescence
Wafer Flatness	Capacitance, optical interferometry, AFM
Epi Layer Thickness	FTIR, capacitance-voltage
Junction Depth	Carrier illumination, modulated photoreflectance
Implant dose	Modulated photoreflectance (thermawave)
Surface Impurities	Total reflection X-ray fluorescence, time-of-flight-SIMS, inductively coupled plasma-mass spectrometry (ICP-MS)
Surface Particles	Surface scattering, SEM/EDS, Raman
Bulk Impurities	Microwave-photoconductance decay, surface photovoltage, photoluminescence
Bulk Lifetime	μW-PCD, surface photovoltage, corona charge, quasi-steady-state photoconductance, free carrier absorption
Surface/Oxide Charge	Corona charge, surface charge analyzer
Insulator Thickness	Ellipsometry, optical reflectivity, X-ray photoelectron spectroscopy, corona charge/Kelvin probe
Critical Dimensions	SEM, scatterometry, spectral ellipsometry, X-ray scattering
Crystal Defects	X-ray topography, polariscopy
Stress	Raman spectroscopy, polariscopy
Temperature	Raman spectroscopy, liquid crystal, scanning thermal probe, pyrometer
Dielectric/Metal Voids	Positron annihilation spectroscopy, acoustic microscopy
Electromigration	X-ray microscopy
Metal Thickness	Picosecond ultrasonics, X-ray reflectometry, X-ray fluorescence, Rutherford backscattering, optical illumination, impulsive stimulated scattering
Dielectric Porosity	X-ray scattering, ellipsometry, neutron scattering, positron annihilation spectroscopy

Some Techniques

Resistivity, Doping Density

Capacitance-Voltage While doping density in polished wafers is not commonly measured, profiling of epitaxial wafers is routinely carried out. It is advantageous to use contactless techniques for this purpose so that the wafer does not have to be sacrificed. A contactless capacitance doping profiling measurement technique uses a contact held in close proximity to the semiconductor wafer. An independently biased guard electrode surrounds the 1 mm diameter sensor electrode, coated with a high dielectric strength thin film. The sensor electrode is held above the wafer by a porous ceramic air bearing, which provides for a very stable distance from the wafer as long as the load on the air bearing does not change, shown in Fig. 1. Pressurizing a bellows provides the controlled load. As air escapes through the porous surface, a cushion of air forms on the wafer that acts like a spring and prevents the contact from touching the wafer. The porosity and air pressure are designed such that the sensing contact floats approximately 0.5 μm above the wafer surface. A stainless steel bellows acts to constrain the pressurized air and to raise the porous disk when the air pressure is reduced. If the air pressure fails, the disk moves up, rather than down to prevent damaging the wafer.[1]

To prepare the wafer, it is placed in a low-concentration ozone environment at a temperature of about 450°C. The treatment reduces the surface charge on the wafer, especially critical for *n*-Si, makes it more uniform, reduces the surface generation velocity and allows deeper depletion.[2] A recent comparison of epitaxial resistivity profiles by this contactless method with Hg-probe *C-V* measurements compared very favorably.[3] The system measures the capacitance from the wafer chuck to the electrode. The capacitance of the air gap is measured by biasing the semiconductor surface in accumulation. Light is used to collapse any possible space-charge region due to surface charge while the sensor is lowered and while the air gap modulation due to the electrostatic attraction is determined to eliminate any series space-charge capacitance. Assuming that the air gap does not vary with changing electrode voltage, the capacitance of the air gap is the measured capacitance at its maximum value. The doping density profile is determined from the conventional *C-V* expressions.[4] Figure 1 shows a resistivity profile, determined from *C-V* data, of a *p*-type Si epitaxial layer on a p^+ substrate.

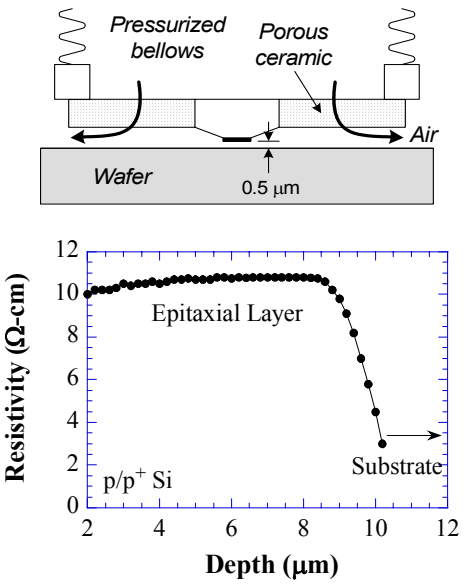

Fig. 1 Contactless doping profiling arrangement and resistivity profile of a p/p^+ Si wafer. Data courtesy of M. Rommel, Semitest.

Minority Carrier Lifetime

Quasi-Steady-State Photoconductance An important addition to the array of minority carrier lifetime characterization tools, is the quasi steady-state photoconductance (QSSPC) instrument.[5] In this method the sample is illuminated with a "slow" flash lamp having a decay time of several ms and an illumination area of several cm^2, which can be reduced to several mm^2 with a light pipe. Due to the slow decay time, the sample is under quasi steady-state conditions during the measurement as the light intensity varies from its maximum to zero. The steady-state condition is maintained as long as the flash lamp decay time is longer than the effective carrier lifetime.

For a *p*-type semiconductor with steady state or transient light incident on the sample, solving the continuity equation for uniform electron-hole pair (ehp) generation and zero surface recombination gives the effective lifetime

$$\tau_{eff}(\Delta n) = \frac{\Delta n(t)}{G(t) - d\Delta n(t)/dt} \qquad (1)$$

where $\Delta n(t)$ is the time-dependent excess minority carrier density and G the ehp generation rate. In the *transient* photoconductance decay (PCD) method, with $G(t) << d\Delta n(t)/dt$

$$\tau_{eff}(\Delta n) = -\frac{\Delta n(t)}{d\Delta n(t)/dt} \qquad (2)$$

In the *steady-state* method, with $G(t) >> d\Delta n(t)/dt$

$$\tau_{eff}(\Delta n) = \frac{\Delta n}{G} \qquad (3)$$

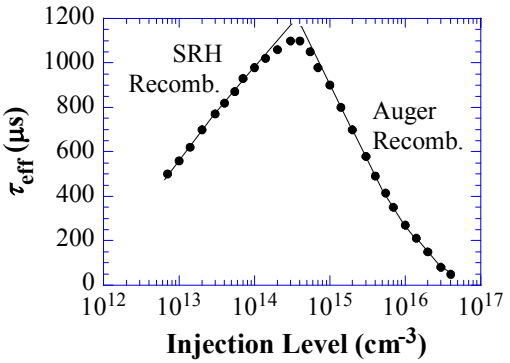

Fig. 2 Effective lifetime versus carrier density. Data after ref. 6.

and in the quasi steady-state photoconductance method, Eq. (1) obtains. Both Δn and G need to be known in the steady state and QSSPC methods to determine the effective lifetime. The effective lifetime is determined by bulk and surface lifetimes.[4] The QSSPC lifetime is shown in Fig. 2 as a function of injection level. As the injection level increases, the lifetime also increases and eventually decreases due to Auger recombination. The important point is that this measurement is done in one flash lamp decay.

Free carrier absorption A novel carrier lifetime characterization approach uses infrared (IR) radiation from a black body transmitted through the semiconductor wafer and detected by an infrared light detecting charge-

coupled device as the detector (mercury-cadmium-telluride or AlGaAs/GaAs).[7] The black body source can be as simple as a hot plate. A laser with $h\nu > E_G$ creates electron-hole pairs in the sample. By taking the difference of the IR radiation through the sample with and without the laser, one measures the *free carrier absorption* due to the excess carriers. Taking two-dimensional images of the IR radiation over the entire wafer, allows for rapid measurements. The system is calibrated with a set of Si wafers of varying doping densities. The transmissivity of these wafers successively placed between the camera and the black body is measured. The signal differences are then due to the differences in free-carrier absorption of the samples. One needs to apply a correction to account for the fact that in the calibration procedure of *p*-type wafers only the IR absorption of holes is measured while in an actual measurement laser-generated electron hole pair generation must be considered.

Knowing the laser generation rate G' ($cm^{-2}s^{-1}$) and the sample thickness d, the effective lifetime is

$$\tau_{eff} = \frac{d\Delta n}{G'} \qquad (4)$$

where $G'=(1-R)\Phi$, with R the reflectivity and Φ the photon flux density. A two-dimensional lifetime map obtained in 50 s with this technique is shown in Fig. 3. No scanning is required, since both black body and excitation laser are broad area sources, covering the entire sample. The black body emits over a wide wavelength range with the peak wavelength at

$$\lambda_{peak} \approx \frac{3000}{T} \ \mu m \qquad (5)$$

Hence, a hot plate at T=350 K, has its peak wavelength at $\lambda_{peak}\approx 8.6$ µm - a very suitable wavelength for free carrier absorption measurements. Just as carriers absorb IR radiation, they also emit IR radiation. According to Kirchhoff's law they emit the same power as they absorb to remain at a given temperature. Hence, if the black body is cooled not to radiate, the sample itself will emit IR radiation and can be used to determine the lifetime. The sample is still excited with a laser and the difference signal is acquired as in the transmission system. Both emission and absorption have been used for lifetime measurements.[8]

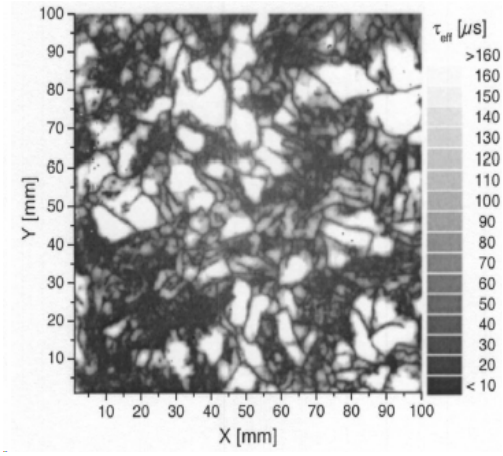

Fig. 3 Free carrier absorption minority carrier lifetimes of a multicrystalline Si wafer with 350 µm lateral resolution. After Isenberg et al. ref. 7.

Photoluminescence Photoluminescence (PL) is most commonly used at low temperatures for impurity identification and for determining low doping densities ($N_{A,D} \le 10^{12}$ cm^{-3}) in Si.[9] Recently, a PL-based commercial tool, SiPHER, has been introduced, operating at room temperature with two wavelengths λ = 532 nm and 827 nm.[10] It measures PL and the optical reflectance and has found application to detect defects (dislocations, oxygen precipitates) and doping density striations in silicon wafers.[11] We make use of the fact that the instrument provides PL and reflectance data at two wavelengths for each measurement point to determine the surface recombination velocity s_r and impurity density N_T.

We have developed one-, two- and three-dimensional models of the carrier distribution in semiconductors following light excitation and use these distributions to calculate PL signals to extract the various doping density and recombination components, predicting the dependence on impurity density and surface recombination velocity in Fig. 4. To determine s_r, we measure PL and optical reflectance at the two exciting laser wavelengths. The PL signal ratio is given by

$$R_{PL} = \frac{PL_{827}}{PL_{532}} = \frac{\Phi_{827}(1-R_{827})F_{827}}{\Phi_{532}(1-R_{532})F_{532}} \qquad (6)$$

where F is a function of the doping concentration, L_n, s_r, and sample reflectivity R. From the measured reflection data and calculated reflectivities, the ratio $\Phi_{827}(1-R_{827})/\Phi_{532}(1-R_{532})$ is

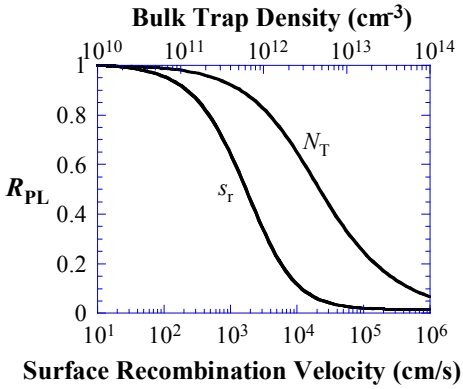

Fig. 4 Normalized PL intensity versus bulk trap density and front surface recombination velocity.

obtained. This leaves only F as the unknown. It depends on B, $p_{o,}$ α, d, L_n and s_r. Hence, R_{PL} depends on N_A, L_n, and s_r with the other parameters known. We calculate R_{PL} versus s_r, as shown in Fig. 4, since we know that PL depends sensitively on s_r. From the experiments we determine R_{PL} and from the R_{PL}-s_r curves, we then determine s_r. For a precise determination of s_r, L_n needs be to be known and can be measured independently. However, since L_n variations for high L_n materials have a relatively small effect on the R_{PL}-s_r curves, an educated L_n guess is sufficient for a reasonably accurate s_r determination. For heavily doped wafers, the lifetime is determined by Auger recombination and knowing the doping concentration allows L_n to be calculated.

Placing the experimental R_{PL} data on these curves, yields s_r = 500-50,000 cm/s for oxidized to bare wafers. The lowest s_r of 500 cm/s is for the oxidized arsenic-doped n-type wafer. The diffusion length for the heavily doped ($N_D = 10^{19}$ cm^{-3}) wafer in Fig. 5 was calculated from known Auger recombination coefficients.

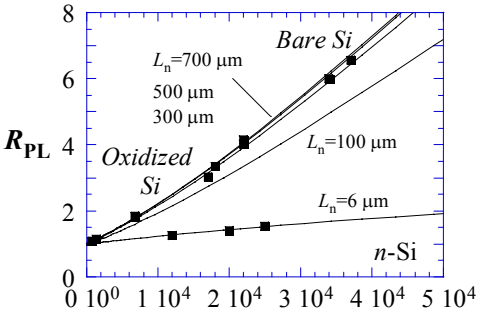

Fig. 5 Theoretical (lines) and experimental (points) PL intensity ratio versus front surface recombination velocity s_r as a function of diffusion length. The high L_n data are for N_A and N_D around 10^{15} cm^{-3}. The "L_n=6 µm" line and data are for N_D=10^{19} cm^{-3}.

Stress

Raman Spectroscopy When light is scattered from the surface of a sample, the scattered light is found to contain mainly wavelengths that are incident on the sample (*Raleigh* scattering) but also at different wavelengths at very low intensities (few parts per million or less) that represent an interaction of the incident light with the material. The interaction of the incident light with optical phonons is called *Raman* scattering while the interaction with acoustic phonons results in *Brillouin* scattering. Optical phonons have higher energies than acoustic phonons giving larger photon energy shifts. For example, the optical phonon energy in Si is about 0.067 eV, while the exciting photon energy is several eV (Ar laser light with λ = 488 nm has an energy of $h\nu$ = 2.54 eV). If the incident photon imparts part of its energy to the lattice in the form of a phonon (phonon emission) it emerges as a lower-energy photon. This down-converted frequency shift is known as *Stokes-shifted* scattering.

Various properties of a sample can be characterized by Raman spectroscopy, which is sensitive to crystal structure, composition, stress, and temperature. Damage and structural imperfections induce scattering by the forbidden TO phonons, allowing implant damage to be monitored, for example. The Stokes line shifts, broadens and becomes asymmetric for microcrystalline Si with grain sizes below 100 Å.[12] The lines become very broad for amorphous semiconductors, allowing a distinction to be made between single crystal, polycrystalline, and amorphous materials. The frequency is also shifted by stress and strain in thin films, as shown in Fig. 6, where the Raman spectra are shown for SiGe films grown on Si substrates. The Si reference signal occurs at $1/\lambda \approx 520$ cm^{-1} and the peak is shifted to lower energies as the Ge fraction increases. Since the SiGe layers are usually very thin, it is important that the exciting laser be absorbed within that thin layer, using an ultraviolet laser.

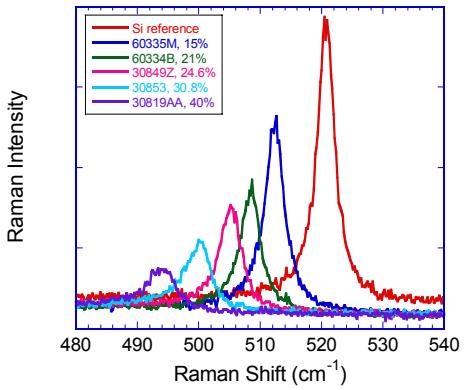

Fig. 6 Raman spectra of Si and $Si_{1-x}Ge_x$/Si (x=0.15 to 0.4). Courtesy of R. Liu, Motorola.

Polariscopy

When a transparent material is subject to mechanical stress, the strain may change the refractive index of the material. This property of transparent materials is called *photoelasticity* and is widely used to determine distributions of stresses or strains in materials. When a stress is applied to an elastic medium, the produced strain is linearly related to stress. If a transparent material is optically isotropic in the absence of stress, the material becomes optically anisotropic by the application of a uniaxial stress. The transmission of light in such anisotropic media has some unique features not present in isotropic materials. When a uniaxial stress is uniformly applied to an optically isotropic material so that the direction of the stress lies in the plane of the sheet, a plane-polarized light ray

is broken up into two components - the *ordinary wave* and the *extraordinary wave.* These waves have polarization vectors at right angles to each other, corresponding to the principal stresses created by the uniaxial stress, and they have different velocities. The ordinary wave has the polarization vector perpendicular and the polarization vector of the extraordinary wave is parallel to the direction of the stress. Since the two components propagate in the medium with different velocities, a phase difference δ is produced between the two components upon emerging from the sheet that is proportional to the magnitude of the shear stress.

The magnitude of δ can be observed by passing the emergent light through an *analyzer.* The principal plane of the analyzer is usually placed at right angles to the polarizer. The two wave components, upon emerging from the analyzer, are reduced into one plane and give rise to interference. When $\delta = (2m+1)\pi$, where *m is* an arbitrary integer, constructive interference takes place and one may see the brightest field of view. When $\delta = 2m\pi$, the interference becomes destructive and the field becomes dark. In general, δ may take any value depending on the actual shear stress in the medium. If there is a distribution of stresses (or strains) in a medium, bright and dark fringes will be seen, and these fringes are contours of equal shear stress. The magnitude of the shear stress can be calculated from the interference order of the fringes. When the polarization vector of the incident light is parallel to one of the principal stresses, the interference fringes disappear and the field of view becomes dark. Thus, the orientation of the principal stresses can be found by rotating the crossed polarizer and analyzer, allowing the distribution of the shearing stress to be determined.

Polariscopy is a nondestructive, highly sensitive and quantitative mapping technique for residual strains in semiconductor wafer.[13] The experimental arrangement for a plane polariscope is schematically shown in Fig. 7. For transmission semiconductor stress measurements, light with $h\nu < E_G$ is used. The infrared light passes through the polarizer and becomes circularly polarized. As light propagates through the silicon, residual stress-induced birefringence changes it from circularly to elliptically polarized. The resulting phase shifts affect the polarization state of transmitted light waves. The intensity of polarization transmission is[14]

$$I_t = I_i(1-R)^2(\cos^2\chi - \sin 2(\phi-\theta)\sin 2(\phi-\theta+\chi)\sin^2\delta/2) \quad (7)$$

where I_i is the intensity of incident light, R the reflectivity, θ the principal angle that determines the orientation of the stress axis at the plane, χ the angle between polarizer and analyzer and ϕ the azimuth angle of the polarizer, shown in Fig. 7. The polarization intensity I measured at selected orientations of the polarizer and analyzer, depends on the optical retardation parameter δ, which, in turn, is directly related to the value of the residual elastic strain.

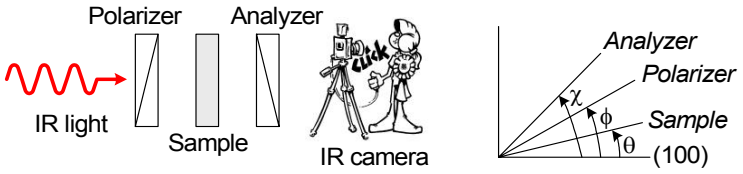

Fig. 7 Plane polariscope.

I_i is generally polarization dependent. Hence a method that does not require I_i and R is desirable. Two transmitted intensities of the polarized light are measured: one with polarizer and analyzer parallel to each other, $I_{\parallel}(\chi = 0)$, and the second with the polarizer orthogonal to the analyzer, $I_{\perp}(\chi = \pi/2)$. By measuring the angular ϕ-dependence of the current ratio one can determine quantitatively both the optical retardation, δ, and the direction of the principal stress angle, θ, using the equation

$$\frac{I_{\perp}}{I_{\perp}+I_{\parallel}} = \sin^2(\phi-\theta)\sin^2(\delta/2) \quad (8)$$

allowing stress to be determined. Example polariscopy images of stressed Si wafers are shown in Fig. 8.

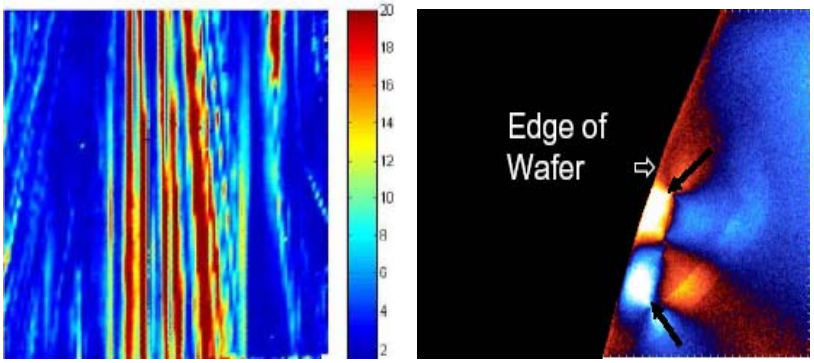

Fig. 8 Residual stress in EFG Si wafer, Courtesy of S. Ostapenko, Univ. of South Florida; stress induced by a small crack in a Si wafer, Courtesy of J. Lesniak, Stress Photonics.

Temperature

High spatial resolution temperature can be measured with Raman spectroscopy, since temperature changes the optical phonon energy leading to a shift in the scattered phonon's energy, shown in Fig. 9. The shift for Si

is –0.021 cm^{-1}/K. Since the Raman laser can be focused to a small spot size, one can make high-resolution temperature measurements on semiconductor devices this way.

Fig. 10(a) shows the temperature along the width of a Si MOSFET clearly illustrating the non-uniform temperature distribution in the width direction.[15] The device runs hotter in the center than along the edges. Fig. 10(b) shows the local temperature near the drain-gate region of AlGaN/GaN power heterojunction FETs on sapphire and SiC substrates.[16] The higher thermal conductivity of SiC clearly lowers the local device temperature and Raman spectroscopy allows such measurements to be made at high spatial resolution.

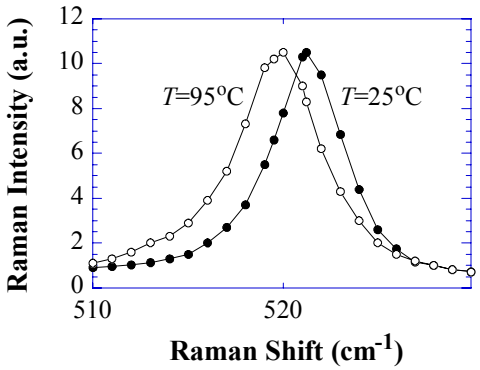

Fig. 9 Raman shift of a MOSFET at T=25°C and 95°C. The 95°C peak is broadened and shifted to lower energies. Adapted from ref. 15.

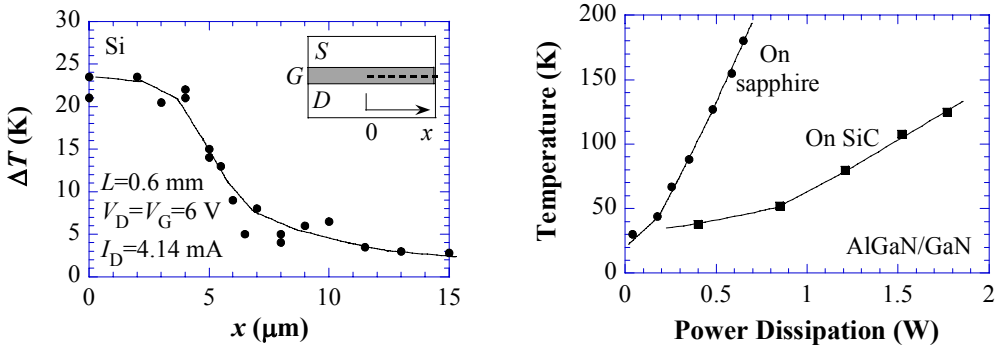

Fig. 10(a) Temperature change profile along the Si MOSFET width direction (from ref. 15), (b) temperature versus power dissipation in the drain-gate region in AlGaN/GaN power HFETs (from ref. 16).

Spectroscopic Ellipsometry

Ellipsometry, a contactless, non-invasive technique measures changes in the polarization state of light reflected from a surface. Spectroscopic ellipsometry (SE) has extended the range of conventional ellipsometry by using more than one wavelength.[17] Furthermore it is possible to vary not only the wavelength but also the angle of incidence, providing yet another degree of freedom. The ellipsometer is sensitive to surface changes on the order of a monolayer. Film thickness and alloy composition can be determined during growth or during etch. Optical measurements are ideal for real-time measurements because they are non-invasive and can be used in any transparent ambient including ambients associated with plasma processing and chemical vapor deposition.

Film Thickness Spectroscopic ellipsometry is one of few techniques allowing thickness measurements of Si films of SOI wafers. Si films as thin as 10 nm can be reliably measured, as shown in Fig. 11, where strained Si on insulator (SSOI) substrates are fabricated by bonding and layer transfer of strained Si layers from SiGe virtual substrates directly to oxidized handle wafers.[18] In this process, the starting strained Si substrates utilize graded SiGe buffer technology to fabricate the high quality relaxed SiGe template to introduce strain in the Si layer. Then, the strained Si wafers are bonded to a handle wafer with an intermediate oxide layer, and the strained Si layer is transferred by hydrogen-induced separation or grind and etch back.

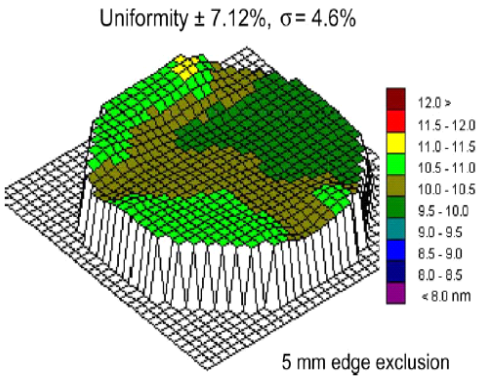

Fig. 11 A 10 nm, 20% strain SSOI strained Si thickness map. After ref. 18.

Ge contents of between 20% and 30% yield tensile Si strain levels between 0.8% and 1.2% and substrates are referred to as 20% SSOI and 30% SSOI, where the 20% and 30% refer to the approximate Ge content of the bulk strained Si substrates from which the strained Si layers were transferred.

Critical Dimensions The use of angle-resolved laser scattering from grating structures is used for dimensional measurements. The use of this concept for deep submicron metrology was pioneered by McNeil and co-workers.[19] They termed this measurement *scatterometry*. The scattered/diffracted light depends on the structure and composition of the features. In a strict physical sense, this light 'scattered' from a periodic sample is due to *diffraction*, but it is termed *scatter*. The manner in which light is scattered from periodic features is sensitive to the geometry of the scattering features. Scatterometry has been used for the measurement of critical dimensions (CDs) and profile characterization of photoresist, poly-silicon and metals. It has also been applied to focus control and lithography tool qualification applications. Because the technique is rapid, non-destructive and has demonstrated excellent precision, it is an attractive alternative to other metrologies used in mainstream semiconductor manufacturing.

Scatterometry can be divided into two parts: the "forward problem" and the "inverse problem".[20] The "forward problem" is the process by which a scatter signature is measured, when the grating is illuminated with a light source and the light is detected with an optical detection system to determine the signature. In the angular technique, the incident angle is varied to obtain the scatter signature. The resulting measurement acts as a "signature" for the scattering features. In the "inverse problem" the geometry of the scattering structure is quantified. Several different approaches have also been explored for the solution of the inverse problem. The most common methods are model-based analyses with the optical scatter data compared to simulations from a theoretical model. The model has been used *a priori* to generate a series of signatures that correspond to discrete iterations of various grating parameters, such as its thickness and the width of the grating lines. The resulting signature is known as a signature "library" or database. The parameters of the modeled signature that agree most closely with the measured signature are taken to be the parameters of this measured signature.

Angle-resolved laser scattering requires reflectometry and/or ellipsometry measurements over a wide range of angles of incidence and reflection and is poorly suited for *in situ* applications and is relatively slow for *ex situ* applications. However, measurement of specular mode reflected light from defined grating structures can be analyzed with accurate diffraction modeling algorithms to yield dimensional information with sub-wavelength resolution. Fixed angle SE or spectral reflectance measurements from period structures show strong promise for high-speed topography measurements. In many cases, SE-based scatterometry measurement have proven to be more detailed and more accurate than top-down scanning electron microscopy and this method is being deployed as an in-line process control tool in the Si IC industry.

For topography extraction, SE or spectral reflectance information is collected from a sample with a one-dimensional grating. The reflection problem from the grating is modeled using high-accuracy numerical simulation of Maxwell's equations. Either a pattern matching procedure using a large, pre-simulated library of line shapes or a parameterized non-linear regression procedure is used to find the best fit between theory and experimental reflection data.[21] Figure 12 shows one component ($\cos 2\Psi$) of the ellipsometric signal for a photoresist grating before and after slight etching. Note the good agreement between theory and experiment. Also note the significant change of the signal after a modest etch. The schematic cross sections show the two lines as modeled and the cross-sectional SEM micrographs show the actual lines. The two agree very well.

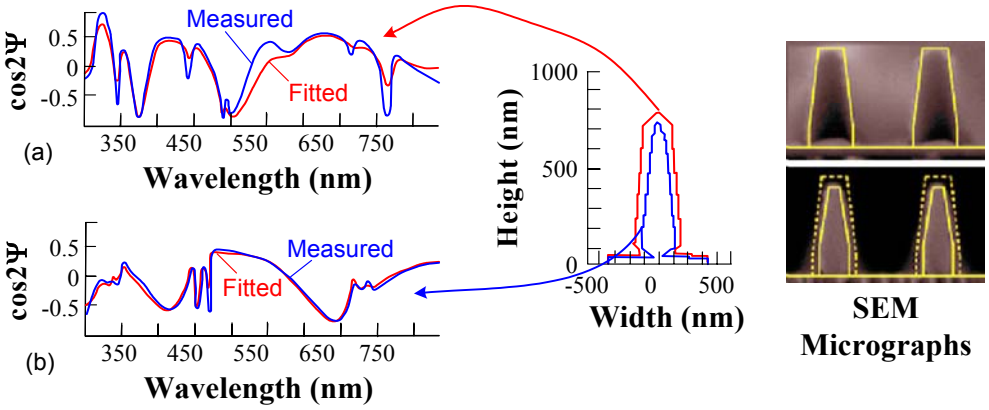

Fig. 12 Measured and fitted SE data and the extrapolated line shape before and after etching. Also shown are SEM micrographs of the lines. After ref. 21.

References

[1] G.G. Barna, B. Van Eck, and J.W. Hosch, in *Handbook of Silicon Semiconductor Technology* (A.C. Diebold, ed.), Dekker, New York (2001), 601.

[2] M. Rommel, Semitest Inc., private correspondence.

[3] K. Woolford, L. Newfield, and C. Panczyk, *Micro*, (2002) (www.micromagazine.com).

[4] D.K. Schroder, *Semiconductor Material and Device Characterization*, 2nd Ed., Wiley-Interscience, New York, 1998.

[5] R.A. Sinton and A. Cuevas, *Appl. Phys. Lett*. **69** (1996) 2510.

[6] M.J. Kerr, A. Cuevas, and R.A. Sinton, "Generalized Analysis of Quasi-Steady-State And Transient Decay Open Circuit Voltage," *J. Appl. Phys*. **9**1, 399-404, Jan. 2002.

[7] M. Bail, J. Kentsch, R. Brendel, and M. Schulz, *Proc. 28th IEEE Photovolt. Conf*. (2000) 99; R. Brendel, M. Bail, B. Bodmann, J. Kentsch, and M. Schulz, *Appl. Phys. Lett.* **80** (2002) 437; J. Isenberg, S. Riepe, S.W. Glunz, and W. Warta, *J. Appl. Phys.* **93** (2003) 4268.

[8] M.C. Schubert, J. Isenberg, and W. Warta, *J. Appl. Phys.* **94** (2003) 4139.

[9] M. Tajima, T. Masui, T. Abe and T. Iizuka, in *Semiconductor Silicon 1981* (H.R. Huff, R.J. Kriegler and Y. Takeishi, eds.) Electrochem. Soc., Pennington, NJ (1981) 72.

[10] SiPHER, Accent Optical Technologies, http://www.accentopto.com.

[11] A. Buczkowski, B. Orschel, S. Kim, S. Rouvimov, B. Sneqirev, M. Fletcher, and F. Kirscht, *J. Electrochem. Soc*. **150** (2003) 436.

[12] H. Richter, Z.P. Wang and L. Ley, *Solid State Commun.* **39** (1981) 625.

[13] S.R. Lederhandler, "Infrared Studies of Birefringence in Silicon," *J. Appl. Phys.* **30** (1959) 1631; R.O. DeNicola and R.N. Tauber, *J. Appl. Phys.* **42** (1971) 4262.

[14] M. Yamada, *Appl. Phys. Lett*. **47** (1985) 365; S. Ostapenko, I. Tarasov, J.P. Kalejs, C. Haessler, and E-U Reisner, *Semicond. Sci. Technol*. **15** (2000) 840.

[15] R. Ostermeir, K. Brunner, G. Abstreiter, and W. Weber, *IEEE Trans. Electron Dev.* **39** (1992) 858.

[16] M. Kuball, J.M. Hayes, M.J. Uren, T. Martin, J.C.H. Birbeck, R.S. Balmer, and B.T. Hughes, *IEEE Electron Dev. Lett.* **23** (2002) 7.

[17] D.E. Aspnes, *Soc. Photoinstrum. Eng.* **946**, 84 (1988).

[18] T.A. Langdo, M.T. Currie, Z.-Y. Cheng, J.G. Fiorenza, M. Erdtmann, G. Braithwaite, C.W. Leitz, C.J. Vineis, J.A. Carlin, A. Lochtefeld, and M.T. Bulsara, I. Lauer, D.A. Antoniadis, and M. Somerville, *Solid-State Electron*. **48** (2004) 1357.

[19] S.A. Coulombe, A.B.K. Minhas, C.J. Raymond, S.S.H. Naqvi, and J.R. McNeil, *J. Vac. Sci. Technol.* **B16** (1998) 80.

[20] C.J. Raymond in *Handbook of Silicon Semiconductor Technology* (A.C. Diebold, ed.), Dekker, New York, (2001) 477

[21] H-T Huang and F.L. Terry, Jr., *Thin Solid Films*, **455/456** (2004) 828.